PTEP

Prog. Theor. Exp. Phys. **2023** 013B07(16 pages)
DOI: 10.1093/ptep/ptac174

IYBSSD2022
International Year
of Basic Sciences
for Sustainable Development

# Precision $\mu^+\mu^+$ and $\mu^+e^-$ elastic scatterings

Yu Hamada[1], Ryuichiro Kitano[1,2], Ryutaro Matsudo[1,3,*], and Hiromasa Takaura[1]

[1]*KEK Theory Center, Tsukuba 305-0801, Japan*
[2]*Graduate University for Advanced Studies (Sokendai), Tsukuba 305-0801, Japan*
[3]*Department of Physics, Taiwan University, Taipei 10617, Taiwan*
*E-mail: matsudo@phys.ntu.edu.tw

Received October 25, 2022; Revised December 7, 2022; Accepted December 17, 2022; Published December 20, 2022

The expected measurement precisions of elastic scattering cross sections are estimated for $\mu^+\mu^+$ and $\mu^+e^-$ colliders, which have recently been proposed as future realistic possibilities ($\mu$TRISTAN). Compared with contributions from possible new physics represented by higher-dimensional operators, we find that the measurements at a TeV energy $\mu^+\mu^+$ collider can probe the scale of new physics up to $O(100)$ TeV. A $\mu^+e^-$ collider for the Higgs boson factory can also improve the electroweak precision test. For those studies, we assume the expected integrated luminosity at $\mu$TRISTAN, $L_{\rm int} = 120\ {\rm fb}^{-1}$ ($\mu^+\mu^+$) and $1\ {\rm ab}^{-1}$ ($\mu^+e^-$).

Subject Index B40, B57, C21

## 1. Introduction

The technology of particle accelerators has made impressive progress since Van de Graaff and Cockcroft–Walton in the early 20th century. The energy frontier has now reached the center-of-mass energy of $O(10)$ TeV for hadron collisions, but even higher energies are demanded by particle physics.

An important task in future accelerator experiments will be to gather information on new physics that enables us to construct guidance for the big picture. In particular, at lepton colliders, well-defined initial states provide a clean environment for precision tests of scattering processes. Indeed, $e^+e^-$ colliders such as the LEP experiments at CERN have provided important inputs towards the complete picture of the Standard Model (SM) [1–3]. In addition, precision tests of the scattering processes have been placing severe constraints on the contributions of new physics [4–10].

The establishment of the SM, at least of its particle content and its gauge group, means that one can now parametrize the effects of physics beyond the SM as coefficients of higher-dimensional operators in the Lagrangian of the Standard Model effective field theory (SMEFT) [11–14]. Although there are possibilities of having light new particles, new physics models motivated by the UV origin of the Higgs boson can generically fall into this type where new particles and/or new interactions appear on the TeV or multi-TeV scale. When a new lepton collider is to be built, the simplest and also one of the most important questions is how well such


Funded by SCOAP[3]. SCOAP[3] and OUP support the goals of the International Year of Basic Sciences for Sustainable Development

coefficients can be measured. At lepton colliders, there are an enormous number of elastic scattering events, which typically have a sharp peak in the forward region. The new physics effects interfere with the SM amplitude and modify the angular distribution mostly in the central region. Such anomalous distributions can be detected with high accuracy and thus provide good probe of microscopic physics. Indeed, prospects at the ILC experiments have been studied, and significant improvement over the current limits has been reported [15,16].

Recently, a new collider experiment, $\mu$TRISTAN [17], using the ultra-cold muon [18], has been proposed. The technology of $\mu^+$ cooling by laser ionization of the muonium (the $\mu^+e^-$ bound state) has been developed for the muon $g-2$/EDM experiment at J-PARC [19]. This technology enables us to consider realistic $\mu^+e^-$ and $\mu^+\mu^+$ colliders. A 3-km storage ring design has the possibility to accelerate $\mu^+$ and $e^-$ beams up to 1 TeV and 30 GeV, respectively, with which $\mu^+e^-$ and $\mu^+\mu^+$ colliders with center-of-mass energies of 346 GeV and 2 TeV can be realized. The luminosities are estimated to be at the level of $10^{33-34}$ cm$^{-2}$ s$^{-1}$, at which the $\mu^+e^-$ collider can be a good Higgs boson factory, whereas direct new particle searches are possible at the high-energy $\mu^+\mu^+$ collider.

In this paper, we examine how well $\mu$TRISTAN can measure the elastic $\mu^+e^-$ and $\mu^+\mu^+$ scattering processes. Since the contributions from, for example, four-fermion operators are larger for higher energies, the $\mu^+\mu^+$ collider at 2 TeV should give the most stringent constraints on the coefficients. We indeed find that the collider can probe the energy scale of $O(100)$ TeV. We include all the SMEFT dimension-six operators that contribute to the elastic scattering. We find that the $\mu^+e^-$ collider at 346 GeV can improve the constraints on the electroweak precision observables such as $S$ and $T$ parameters [20,21]. By assuming ten years of running, the experiments can accumulate integrated luminosity at the level of 120 fb$^{-1}$ ($\mu^+\mu^+$) and 1 ab$^{-1}$ ($\mu^+e^-$) [17]. We use these values for the reference luminosities in this study.

This paper is organized as follows. In Sect. 2, we give a review on SMEFT and specify the operators that we consider. We give the expected constraints on SMEFT operators at a $\mu^+\mu^+$ collider (Sect. 3) and at a $e^-\mu^+$ collider (Sect. 4). We compare our result with the current constraints in Sect. 5. Sect. 6 is devoted to the summary. In Appendix A, we present kinematic formulas relevant to an $e^-\mu^+$ collider, whose beam energies are asymmetric.

## 2. SMEFT Lagrangian

In this section, we present the formulas necessary to calculate scatterings $e^-\mu^+ \to e^-\mu^+$ and $\mu^+\mu^+ \to \mu^+\mu^+$ within SMEFT. This includes a review on the relations between ($\alpha$, $M_Z$, $G_F$) and SMEFT Lagrangian parameters. We consider up to dimension-six operators adopting the basis of Ref. [22]. All calculations in this paper are performed at the tree level.

### 2.1 *Gauge fields*

Let us first consider the Lagrangian for the gauge fields. The following four higher-dimensional operators

$$Q_{HW} = H^\dagger H W^I_{\mu\nu} W^{I\mu\nu} \tag{1}$$

$$Q_{HB} = H^\dagger H B_{\mu\nu} B^{\mu\nu} \tag{2}$$

$$Q_{HWB} = H^\dagger \tau^I H W^I_{\mu\nu} B^{\mu\nu} \tag{3}$$

$$Q_{HD} = (H^\dagger D_\mu H)^*(H^\dagger D_\mu H) \tag{4}$$

are involved assuming CP invariance. The Lagrangian is given by

$$\begin{aligned}
\mathcal{L}_{\text{gauge}} &= -\frac{1}{4}B^{\mu\nu}B_{\mu\nu} - \frac{1}{4}W^I_{\mu\nu}W^{I\mu\nu} + D_\mu H^\dagger D^\mu H \\
&\quad + C_{HW}H^\dagger H W^I_{\mu\nu}W^{I\mu\nu} + C_{HB}H^\dagger H B_{\mu\nu}B^{\mu\nu} + C_{HWB}H^\dagger \tau^I H W^I_{\mu\nu}B^{\mu\nu} \\
&\quad + C_{HD}(H^\dagger D_\mu H)^*(H^\dagger D_\mu H) \\
&= -\frac{1}{4}(1-2v^2C_{HB})B^{\mu\nu}B_{\mu\nu} - \frac{1}{4}(1-2v^2C_{HW})W^3_{\mu\nu}W^{3\mu\nu} - \frac{v^2}{2}C_{HWB}W^3_{\mu\nu}B^{\mu\nu} \\
&\quad + \left(W^3_\mu, B_\mu\right) M \begin{pmatrix} W^3_\mu \\ B_\mu \end{pmatrix} - \frac{1}{2}(1-2v^2C_{HW})W^+_{\mu\nu}W^{\mu\nu-} + \frac{g^2v^2}{4}W^+_\mu W^{\mu-} + \cdots .
\end{aligned} \tag{5}$$

Here we define the matrix $M$ by

$$M = \left(1 + \frac{v^2}{2}C_{HD}\right)\begin{pmatrix} \frac{g^2v^2}{8} & -\frac{gg'v^2}{8} \\ -\frac{gg'v^2}{8} & \frac{g'^2v^2}{8} \end{pmatrix}, \tag{6}$$

and define $W^+ = \frac{1}{\sqrt{2}}(W^1 - iW^2)$ and $W^- = \frac{1}{\sqrt{2}}(W^1 + iW^2)$. In the final equality, we show explicitly only the part where the Higgs vacuum expectation value (VEV) is substituted and the quadratic part in the gauge fields. We use $D_\mu H = (\partial_\mu + i\frac{g}{2}\tau^I W^I_\mu + i\frac{g'}{2}B_\mu)H$ and $\langle H\rangle = \frac{1}{\sqrt{2}}\begin{pmatrix} 0 \\ v \end{pmatrix}$.

Let us consider $A_\mu$ and $Z_\mu$ part, i.e. $B_\mu$ and $W^3_\mu$ part. We can diagonalize the matrix $M$ by

$$\begin{pmatrix} W^3_\mu \\ B_\mu \end{pmatrix} = \begin{pmatrix} \cos\theta_W & \sin\theta_W \\ -\sin\theta_W & \cos\theta_W \end{pmatrix}\begin{pmatrix} Z_\mu \\ A_\mu \end{pmatrix}, \tag{7}$$

where $\cos\theta_W = g/\sqrt{g^2+g'^2}$ and $\sin\theta_W = g'/\sqrt{g^2+g'^2}$. Note that $\theta_W$ differs from the SM value of the Weinberg angle. This is because $g$ and $g'$ are different from their SM values, which are determined by assuming the SM. The mass term turns into

$$\left(W^3_\mu, B_\mu\right) M \begin{pmatrix} W^3_\mu \\ B_\mu \end{pmatrix} = \frac{1}{2}\left(1 + \frac{v^2}{2}C_{HD}\right)\frac{1}{4}(g^2+g'^2)v^2 Z_\mu Z^\mu. \tag{8}$$

Then the kinetic terms are written in the form of

$$\mathcal{L} = -\frac{1}{4}(1+\epsilon_1)F_{\mu\nu}F^{\mu\nu} - \frac{1}{4}(1+\epsilon_2)Z_{\mu\nu}Z^{\mu\nu} + \epsilon_3 F_{\mu\nu}Z^{\mu\nu}. \tag{9}$$

Here the $\epsilon_i$ parameters are given by

$$\epsilon_1 = -2v^2C_{HB}\cos^2\theta_W - 2v^2C_{HW}\sin^2\theta_W + 2v^2C_{HWB}\cos\theta_W\sin\theta_W, \tag{10}$$

$$\epsilon_2 = -2v^2C_{HB}\sin^2\theta_W - 2v^2C_{HW}\cos^2\theta_W - 2v^2C_{HWB}\cos\theta_W\sin\theta_W, \tag{11}$$

$$\epsilon_3 = -v^2C_{HB}\cos\theta_W\sin\theta_W + v^2C_{HW}\cos\theta_W\sin\theta_W - \frac{v^2}{2}C_{HWB}(\cos^2\theta_W - \sin^2\theta_W). \tag{12}$$

After the following (nonorthogonal) transformation

$$\begin{cases} A_\mu \to A_\mu + 2\epsilon_3 Z_\mu \\ Z_\mu \to Z_\mu \end{cases}, \tag{13}$$

the kinetic term becomes

$$\mathcal{L} = -\frac{1}{4}(1+\epsilon_1)F_{\mu\nu}F^{\mu\nu} - \frac{1}{4}(1+\epsilon_2)Z_{\mu\nu}Z^{\mu\nu}, \tag{14}$$

where the kinetic mixing is eliminated. Note that the mass term is invariant under the above transformation because we shift only the zero-mass field. To make the kinetic terms canonical, we need further rescaling by $\sqrt{1+\epsilon_1}$ and $\sqrt{1+\epsilon_2}$ for $A_\mu$ and $Z_\mu$, respectively. As a whole, we should use the following correspondence:

$$\begin{pmatrix} W_\mu^3 \\ B_\mu \end{pmatrix} = \begin{pmatrix} \cos\theta_W & \sin\theta_W \\ -\sin\theta_W & \cos\theta_W \end{pmatrix} \begin{pmatrix} \frac{1}{\sqrt{1+\epsilon_2}} Z_\mu \\ \frac{1}{\sqrt{1+\epsilon_1}} A_\mu + 2\epsilon_3 Z_\mu \end{pmatrix}. \tag{15}$$

Under this understanding the quadratic term of gauge fields becomes

$$\mathcal{L} = -\frac{1}{4}F_{\mu\nu}F^{\mu\nu} - \frac{1}{4}Z_{\mu\nu}Z^{\mu\nu} + \frac{1}{2}\frac{1}{1+\epsilon_2}\left(1+\frac{v^2}{2}C_{HD}\right)\frac{1}{4}(g^2+g'^2)v^2 Z_\mu Z^\mu. \tag{16}$$

At this stage, we obtain a mass for the $Z_\mu$ field

$$M_Z = \sqrt{\frac{1+\frac{v^2}{2}C_{HD}}{1+\epsilon_2}}\sqrt{\frac{1}{4}(g^2+g'^2)v^2} \simeq \left(1+\frac{v^2}{4}C_{HD}-\frac{1}{2}\epsilon_2\right)\sqrt{\frac{1}{4}(g^2+g'^2)v^2}, \tag{17}$$

up to the linear order of the SMEFT operators.

Now we consider $W^\pm$ part. We consider the following redefinition

$$W_\mu^\pm \to \frac{1}{\sqrt{1-2v^2C_{HW}}}W_\mu^\pm \simeq (1+v^2C_{HW})W_\mu^\pm. \tag{18}$$

from which the W boson mass is obtained as

$$M_W^2 = \frac{1}{1-2v^2C_{HW}}\frac{g^2v^2}{4} \simeq (1+2v^2C_{HW})\frac{g^2v^2}{4}. \tag{19}$$

### 2.2 *Interaction Lagrangian for fermions*

The interaction Lagrangian of mass dimension four is given by

$$\begin{aligned}
\mathcal{L}_{\text{dim-4}}^{\text{fermion}} &= \bar{L}i\gamma^\mu\left(\partial_\mu + i\frac{g}{2}\tau^I W_\mu^I - i\frac{g'}{2}B_\mu\right)L + \bar{R}i\gamma^\mu(\partial_\mu - ig'B_\mu)R \\
&= (\text{kin. term}) \\
&\quad + \frac{gg'}{\sqrt{g^2+g'^2}}\left(1-\frac{\epsilon_1}{2}\right)A_\mu\bar{\psi}_L\gamma^\mu\psi_L + \frac{gg'}{\sqrt{g^2+g'^2}}\left(1-\frac{\epsilon_1}{2}\right)A_\mu\bar{\psi}_R\gamma^\mu\psi_R \\
&\quad + \left[\frac{1}{2}\frac{g^2-g'^2}{\sqrt{g^2+g'^2}}\left(1-\frac{\epsilon_2}{2}\right) + 2\epsilon_3\frac{gg'}{\sqrt{g^2+g'^2}}\right]Z_\mu\bar{\psi}_L\gamma^\mu\psi_L \\
&\quad + \left[-\frac{g'^2}{\sqrt{g^2+g'^2}}\left(1-\frac{\epsilon_2}{2}\right) + 2\epsilon_3\frac{gg'}{\sqrt{g^2+g'^2}}\right]Z_\mu\bar{\psi}_R\gamma^\mu\psi_R \\
&\quad - \frac{g}{\sqrt{2}}(1+v^2C_{HW})(W_\mu^+J^\mu + W_\mu^-J^{\mu\dagger}) + \cdots
\end{aligned} \tag{20}$$

Here $\psi$ denotes a charged lepton and $J_\mu = \bar{\nu}_L\gamma^\mu e_L = \bar{\nu}_e\gamma^\mu P_L e + \bar{\nu}_\mu\gamma^\mu P_L\mu$.

The following dimension-six operators

$$\begin{aligned}
Q_{H\ell}^{(1)} &= (H^\dagger i\overleftrightarrow{D}_\mu H)(\bar{L}\gamma^\mu L) = vM_Z Z_\mu(\bar{\psi}\gamma^\mu P_-\psi) + \cdots, \\
Q_{H\ell}^{(3)} &= (H^\dagger i\overleftrightarrow{D}^I_\mu H)(\bar{L}\tau^I\gamma^\mu L) = -vM_Z Z_\mu(\bar{\psi}\gamma^\mu P_-\psi) - \frac{g}{\sqrt{2}}v^2(W_\mu^+J^\mu + W_\mu^-J^{\mu\dagger}) + \cdots, \\
Q_{He} &= (H^\dagger i\overleftrightarrow{D}_\mu H)(\bar{R}\gamma^\mu R) = vM_Z Z_\mu(\bar{\psi}\gamma^\mu P_+\psi) + \cdots,
\end{aligned} \tag{21}$$

further modify the interaction terms. We assume flavor conservation and flavor universality for these operators. There are interesting operators which contribute to the anomalous magnetic

moments such as $\bar{L}\sigma^{\mu\nu}RHF_{\mu\nu}$. However, these operators do not contribute to the scattering processes in the limit of the vanishing muon mass. Therefore, we do not consider these operators in the following discussion. Even though the direct probe of the anomalous magnetic moment is difficult at the scattering processes, the new physics model generically modifies other dimension-six operators. In this sense, the scattering experiment may give some information for the possible solution to the muon $g-2$ anomaly [23–26]. From Eq. (21), we obtain

$$\begin{aligned}\mathcal{L}_{\rm SMEFT}^{\rm fermion} &= (\text{kin. term})\\ &+ \frac{gg'}{\sqrt{g^2+g'^2}}\left(1-\frac{\epsilon_1}{2}\right)A_\mu\bar{\psi}_L\gamma^\mu\psi_L + \frac{gg'}{\sqrt{g^2+g'^2}}\left(1-\frac{\epsilon_1}{2}\right)A_\mu\bar{\psi}_R\gamma^\mu\psi_R\\ &+ \left[\frac{1}{2}\frac{g^2-g'^2}{\sqrt{g^2+g'^2}}\left(1-\frac{\epsilon_2}{2}\right)+2\epsilon_3\frac{gg'}{\sqrt{g^2+g'^2}}+\frac{1}{2}vM_Z\left(C_{H\ell}^{(1)}-C_{H\ell}^{(3)}\right)\right]Z_\mu\bar{\psi}_L\gamma^\mu\psi_L\\ &+ \left[-\frac{g'^2}{\sqrt{g^2+g'^2}}\left(1-\frac{\epsilon_2}{2}\right)+2\epsilon_3\frac{gg'}{\sqrt{g^2+g'^2}}+\frac{1}{2}vM_ZC_{H\mu}\right]Z_\mu\bar{\psi}_R\gamma^\mu\psi_R\\ &- \frac{g}{\sqrt{2}}\left(1+v^2C_{H\ell}^{(3)}+v^2C_{HW}\right)\left(W_\mu^+J^\mu+W_\mu^-J^{\mu\dagger}\right)+\cdots. \end{aligned} \tag{22}$$

From this, the electric coupling constant is obtained as

$$e = \frac{gg'}{\sqrt{g^2+g'^2}}\left(1-\frac{\epsilon_1}{2}\right). \tag{23}$$

In SMEFT, fermions interact also through four-fermion interactions. The ones relevant to our calculations are given by

$$Q_{\substack{\ell\ell\\prst}} = (\bar{\ell}_p\gamma_\mu\ell_r)(\bar{\ell}_s\gamma^\mu\ell_t), \tag{24}$$

$$Q_{\substack{\ell e\\prst}} = (\bar{\ell}_p\gamma_\mu\ell_r)(\bar{e}_s\gamma^\mu e_t), \tag{25}$$

$$Q_{\substack{ee\\prst}} = (\bar{e}_p\gamma_\mu e_r)(\bar{e}_s\gamma^\mu e_t). \tag{26}$$

Here $p$, $r$, $s$, $t$ are flavor indices. The Lagrangian is given by

$$\mathcal{L}_{\text{four-fermi}} = \sum_{p,r,s,t}\left(C_{\substack{\ell\ell\\prst}}Q_{\substack{\ell\ell\\prst}} + C_{\substack{\ell e\\prst}}Q_{\substack{\ell e\\prst}} + C_{\substack{ee\\prst}}Q_{\substack{ee\\prst}}\right). \tag{27}$$

For this Lagrangian, we impose

$$C_{\substack{\ell\ell\\e\mu\mu e}} = C_{\substack{\ell\ell\\\mu ee\mu}} \equiv C_{\ell\ell}. \tag{28}$$

We list the quantities on which we can give constraints via measurements of the scatterings.

$$\begin{aligned} &C_{\substack{\ell\ell\\\mu\mu\mu\mu}}, \quad C''_{\ell\ell} \equiv \frac{1}{2}\left(C_{\substack{\ell\ell\\ee\mu\mu}} + C_{\substack{\ell\ell\\\mu ee\mu}}\right), \quad C_{\substack{\ell e\\\mu\mu\mu\mu}}, \quad C_{\substack{\ell e\\ee\mu\mu}}, \quad C_{\substack{\ell e\\\mu ee\mu}}, \quad C_{\substack{ee\\\mu\mu\mu\mu}},\\ &C_{e\mu} \equiv \frac{1}{4}\left(C_{\substack{ee\\\mu\mu ee}} + C_{\substack{ee\\ee\mu\mu}} + C_{\substack{ee\\\mu ee\mu}} + C_{\substack{ee\\e\mu\mu e}}\right). \end{aligned} \tag{29}$$

Note a Fierz identity $(\gamma_\mu P_s)_{\alpha\beta}(\gamma^\mu P_s)_{\gamma\delta} = -(\gamma_\mu P_s)_{\alpha\delta}(\gamma^\mu P_s)_{\gamma\beta}$. We assume flavor conservation for these operators. Therefore, the $(p, r, s, t) = (\mu, e, \mu, e)$ or $(e, \mu, e, \mu)$ type operator does not exist.

Integrating out the $W$ field in Eq. (22) yields the following four-fermion Lagrangian:

$$\begin{aligned}\mathcal{L} &= -\frac{g^2\left(1+v^2C_{H\ell}^{(3)}+v^2C_{HW}\right)^2}{2M_W^2}J_\mu^\dagger J^\mu+\cdots\\ &= -\frac{g^2\left(1+v^2C_{H\ell}^{(3)}+v^2C_{HW}\right)^2}{2M_W^2}\\ &\quad\times\left[(\bar{\nu}_e\gamma_\mu P_L e)(\bar{\mu}\gamma^\mu P_L\nu_\mu)+(\bar{e}\gamma_\mu P_L\nu_e)(\bar{\nu}_\mu\gamma^\mu P_L\mu)+\cdots\right].\end{aligned} \tag{30}$$

Together with the four-fermion Lagrangian and Eq. (28), we obtain

$$\frac{G_F}{\sqrt{2}}=\frac{1}{2v^2}\left(1+2v^2C_{H\ell}^{(3)}-v^2C_{\ell\ell}\right), \tag{31}$$

where $C_{HW}$ in Eq. (30) has been cancelled by that in $M_W$.

We summarize the important relations.

$$4\pi\alpha=\frac{g^2g'^2}{g^2+g'^2}(1-\epsilon_1), \tag{32}$$

$$M_Z^2=\frac{g^2+g'^2}{4}v^2\left(1+\frac{v^2}{2}C_{HD}-\epsilon_2\right), \tag{33}$$

$$\frac{G_F}{\sqrt{2}}=\frac{1}{2v^2}\left(1+2v^2C_{H\ell}^{(3)}-v^2C_{\ell\ell}\right). \tag{34}$$

The quantities of left-hand side are accurately measured in experiments. We use the following values:

$$\alpha_{EW}=127.95^{-1},\quad M_Z=91.1876\,\text{GeV},\quad G_F=1.16638\times10^{-5}\,\text{GeV}^{-2}. \tag{35}$$

The SM gauge couplings and SM Higgs VEV are determined by setting the dimension-six operator contributions to zero, i.e.

$$4\pi\alpha=\frac{g_{\rm SM}^2g'^2_{\rm SM}}{g_{\rm SM}^2+g'^2_{\rm SM}}, \tag{36}$$

$$M_Z^2=\frac{g_{\rm SM}^2+g'^2_{\rm SM}}{4}v_{\rm SM}^2, \tag{37}$$

$$\frac{G_F}{\sqrt{2}}=\frac{1}{2v_{\rm SM}^2}. \tag{38}$$

The above equations are understood as the (tree-level) definition of $\{g'_{\rm SM}, g_{\rm SM}, v_{\rm SM}\}$. The correct relations when assuming SMEFT are given by Eqs. (32) –(34), and hence we expand $g$, $g'$, and $v$ as $g=g_{\rm SM}+\delta g$, $g'=g'_{\rm SM}+\delta g'$, and $v=v_{\rm SM}+\delta v$, where perturbative corrections $\delta...$ are given by linear combinations of the coefficients of the dimension-six operators. Once we obtain the gauge couplings and VEV in this manner, SMEFT gives nontrivial predictions for physical observables except for $\{\alpha, M_Z^2, G_F\}$. For instance, SMEFT predicts the W boson mass as

$$M_W^2 = (1+2v^2 C_{HW})\frac{g^2 v^2}{4} \tag{39}$$

$$= [1+2\left(v_{\rm SM}^2+\delta v^2\right)C_{HW}]\frac{(g_{\rm SM}+\delta g)^2\left(v_{\rm SM}^2+\delta v^2\right)}{4}$$

$$= M_{W,{\rm SM}}^2\Bigg[1-\frac{1}{2}\frac{\cos^2\theta_{\rm SM}}{\cos^2\theta_{\rm SM}-\sin^2\theta_{\rm SM}}v_{\rm SM}^2 C_{HD}$$

$$-\frac{\sin^2\theta_{\rm SM}}{\cos^2\theta_{\rm SM}-\sin^2\theta_{\rm SM}}v_{\rm SM}^2\left(2C_{H\ell}^{(3)}-C_{\ell\ell}\right)-\frac{2\cos\theta_{\rm SM}\sin\theta_{\rm SM}}{\cos^2\theta_{\rm SM}-\sin^2\theta_{\rm SM}}v_{\rm SM}^2 C_{HWB}\Bigg], \tag{40}$$

where $M_{W,{\rm SM}}^2 = g_{\rm SM}^2 v_{\rm SM}^2/4$, $\cos\theta_{\rm SM} = g_{\rm SM}/\sqrt{g_{\rm SM}^2+(g'_{\rm SM})^2}$. In this paper, we give SMEFT predictions for the elastic scatterings. The calculations are based on the results for $g = g_{\rm SM}+\delta g$, $g' = g'_{\rm SM}+\delta g'$, and $v = v_{\rm SM}+\delta v$ and the Lagrangian Eqs. (22) and (27).

It is often convenient to parameterize contributions from new physics in terms of the oblique $S$ and $T$ parameters [20,21]. They are related to the SMEFT operator within our basis as

$$\frac{v^2}{\Lambda^2}C_{HWB} = \frac{g'g}{16\pi}S, \quad \frac{v^2}{\Lambda^2}C_{HD} = -\frac{g'^2 g^2}{2\pi(g^2+g'^2)}T, \tag{41}$$

which enable us to translate the constraints on the SMEFT operators into those on the electroweak precision observables.

## 3. Precision measurements at a $\mu^+\mu^+$ collider

In this section, we calculate the process $\mu^+\mu^+\to\mu^+\mu^+$ using the SMEFT Lagrangian discussed above. First, we give the SM amplitude. Let $s_1$ and $s_2$ be the polarizations of initial muons. Then the magnitude of the amplitude is given by

$$\sum_{s_3,s_4}|\mathcal{M}_{s_1s_2}^{\rm SM}|^2$$

$$= \sum_{i,j=\gamma,Z} g^i_{-s_1}g^j_{-s_1}g^i_{-s_2}g^j_{-s_2}$$

$$\times\Bigg\{8[(1+s_1s_2)(p_1\cdot p_2)(p_3\cdot p_4)+(1-s_1s_2)(p_1\cdot p_4)(p_2\cdot p_3)]\frac{1}{D_i(p_1-p_3)}\frac{1}{D_j(p_1-p_3)}$$

$$+8[(1+s_1s_2)(p_1\cdot p_2)(p_3\cdot p_4)+(1-s_1s_2)(p_1\cdot p_3)(p_2\cdot p_4)]\frac{1}{D_i(p_1-p_4)}\frac{1}{D_j(p_1-p_4)}$$

$$+16\delta_{s_1s_2}(p_1\cdot p_2)(p_3\cdot p_4)\left[\frac{1}{D_i(p_1-p_3)}\frac{1}{D_j(p_1-p_4)}+\frac{1}{D_i(p_1-p_4)}\frac{1}{D_j(p_1-p_3)}\right]\Bigg\}, \tag{42}$$

where $D_i(p)\equiv p^2-M_i^2$ with $M_\gamma = 0$ and $M_Z\neq 0$. We summed up the spins of the final muons $s_3$ and $s_4$. We denote by $p_1$ and $p_2$ the initial muon momenta and by $p_3$ and $p_4$ those of the final muons. We have

$$p_1\cdot p_2 = p_3\cdot p_4 = \frac{s}{2}, \quad p_1\cdot p_4 = p_2\cdot p_3 = \frac{s}{2}(1-y), \quad p_1\cdot p_3 = p_2\cdot p_4 = \frac{s}{2}y \tag{43}$$

with $y = (1-\cos\theta)/2$. The coupling $g_+^Z$ is defined by

$$\mathcal{L} = g_+^Z Z^\mu \bar\psi\gamma_\mu P_+\psi+\cdots \tag{44}$$

with $P_\pm = (1 \pm \gamma_5)/2$. The other couplings are understood in a similar manner. The total cross section is given by

$$\sigma = \frac{1}{64\pi s}\int_{\theta_{\rm min}}^{\pi-\theta_{\rm min}} d\theta \sin\theta \sum_{s_3,s_4} |\mathcal{M}_{s_1 s_2}|^2. \tag{45}$$

Note that the final particles are identical. We introduced an cutoff to the angular integration. (Otherwise, the total cross section diverges.) Furthermore, we divide the angle range $[\theta_{\rm min}, \pi - \theta_{\rm min}]$ into some bins.

The calculation using the SMEFT Lagrangian (22) requires a slight modification to the SM calculation; it is sufficient to shift the SM coupling constants appropriately. In addition, we have to calculate the four-fermion interaction contribution. We consider the interference between the SM and the four-fermion contribution.

In the following analysis, we turn on one of the dimension-six operator coefficients and study how well we can constrain it through the scattering experiments. We repeat this kind of analysis for all the coefficients. Schematically we can give the cross section integrated over one bin (at $\theta = \theta_i$) as

$$\sigma(\theta_i) = \sigma_{\rm SM}(\theta_i) + \hat{C}\sigma_{\rm NP}(\theta_i). \tag{46}$$

Here $\sigma_{\rm SM}(\theta_i)$ represents the SM cross section, while $\hat{C}\sigma_{\rm NP}(\theta_i)$ represents the contribution from a focused dimension-six operator. $\hat{C}$ is a dimensionless coefficient, $\hat{C} = C \times {\rm TeV}^2$, originating from the dimension-six operator coefficient $C$. The coefficient $\hat{C}$ is determined by a fit in actual experiments using the $\chi^2$-test. Here, we give a constraint on it assuming that no deviation from SM predictions is observed. Then $\chi^2$ is given by

$$\chi^2 = \sum_{i:{\rm bin}} \left[\frac{\hat{C}\sigma_{\rm NP}(\theta_i)}{\Delta\sigma(\theta_i)}\right]^2, \tag{47}$$

where the statistical error on the cross section is assumed to be

$$\Delta\sigma(\theta_i) = \frac{\sigma_{\rm SM}(\theta_i)}{\sqrt{\int \mathcal{L}{\rm d}t \cdot \sigma_{\rm SM}(\theta_i)}}. \tag{48}$$

A two-sigma constraint on $\hat{C}$ can be then obtained as

$$|\hat{C}| < \sqrt{\frac{4}{\sum_{i:{\rm bin}}\left[\frac{\sigma_{\rm NP}(\theta_i)}{\Delta\sigma(\theta_i)}\right]^2}}. \tag{49}$$

We give our constraints in terms of new physics (or cutoff) scales. Namely, we define a new physics scale as

$$C := \frac{1}{\Lambda^2}. \tag{50}$$

Then we obtain the two-sigma constraint for the new physics scale as

$$\Lambda > \left(\frac{4}{\sum_{i:{\rm bin}}\left[\frac{\sigma_{\rm NP}(\theta_i)}{\Delta\sigma(\theta_i)}\right]^2}\right)^{-1/4} {\rm TeV}. \tag{51}$$

We consider the range $16^\circ < \theta < 164^\circ$ and take the bin size as $1^\circ$. For instance, $\sigma(\theta_i = 16^\circ)$ means the cross section integrated over $15.5^\circ < \theta < 16.5^\circ$. The number of bins is 148. The constraint we expect to obtain is given in Table 1 for $\sqrt{s} = 2$ TeV. We assume the integrated luminosity to be 120 fb$^{-1}$. The initial helicity corresponds to R: $s = +1$ and L: $s = -1$. We can

**Table 1.** Constraints on SMEFT operators at the two-sigma level obtained from a $\mu^+\mu^+$ collider at $\sqrt{s} = 2$ TeV. The integrated luminosity is assumed to be 120 fb$^{-1}$. The polarization of the $\mu^+$ beams is taken to be purely right- or left-handed as indicated in the table. The bin size for $\theta$ is taken as $1^\circ$ and each bin covers the range $\theta_i - 0.5^\circ < \theta < \theta_i + 0.5^\circ$. The considered range of $\theta_i$ is $16^\circ \le \theta_i \le 164^\circ$.

| | RR | LL | RL |
|---|---|---|---|
| $C_{HWB}$ | 10 TeV | 9.4 TeV | 2.3 TeV |
| $C_{HD}$ | 5.5 TeV | 3.5 TeV | 2.3 TeV |
| $C_{H\ell}^{(1)}$ | 8.0 TeV | 0 | 4.9 TeV |
| $C_{H\ell}^{(3)}$ | 14 TeV | 7.0 TeV | 6.7 TeV |
| $C_{He}$ | 0 | 7.5 TeV | 5.3 TeV |
| $C_{\ell\ell}$ | 7.7 TeV | 5.0 TeV | 3.3 TeV |
| $C_{\mu\mu\mu\mu}^{\ell\ell}$ | 100 TeV | 0 | 0 |
| $C_{\mu\mu\mu\mu}^{ee}$ | 0 | 100 TeV | 0 |
| $C_{\mu\mu\mu\mu}^{\ell e}$ | 0 | 0 | 46 TeV |

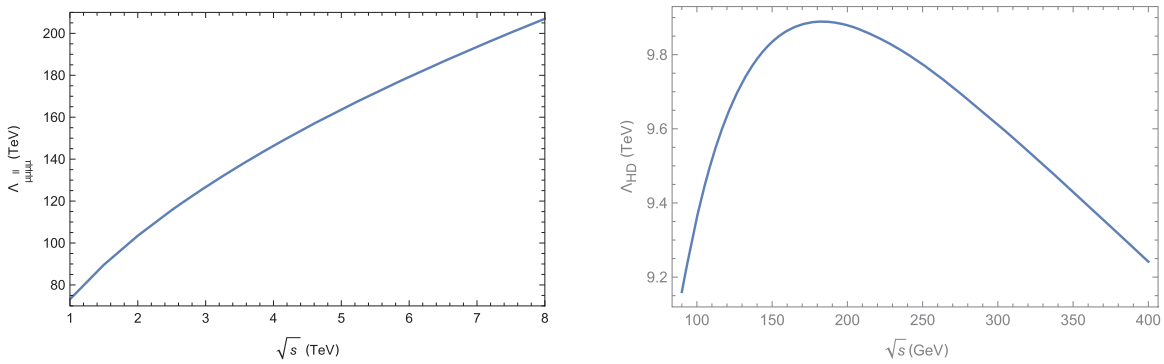


**Fig. 1.** The $\sqrt{s}$ dependence of the bounds on $\Lambda_{\ell\ell,\,\mu\mu\mu\mu}$ (left) and $\Lambda_{HD}$ (right) at the $\mu^+\mu^+$ collider. The initial helicity is set to be $s_1 = s_2 = 1$.

obtain a powerful constraint on four-fermion operators of $\mathcal{O}(100)$ TeV. The $\sqrt{s}$ dependence of the bounds of $\Lambda_{\mu\mu\mu\mu}^{\ell\ell}$ and $\Lambda_{HD}$ is given in Fig. 1.

We need to check whether the $\theta$ dependence of the new physics contribution is different from the SM contribution, because the luminosity would be measured by using the same scattering process. We checked that the ratio of the new physics contribution to the SM one has nontrivial dependence on $\theta$. See Fig. 2.

## 4. Precision measurements at a $\mu^+e^-$ collider

Now we consider the scattering $e^-\mu^+ \to e^-\mu^+$. The SM cross section is given through

$$\sum_{s_3,s_4} \left|\mathcal{M}_{s_1 s_2}^{\rm SM}\right|^2 = \sum_{i,j} g_{s_1}^i g_{s_1}^j g_{-s_2}^i g_{-s_2}^j 8[(1+s_1 s_2)(p_1\cdot p_2)(p_3\cdot p_4) + (1-s_1 s_2)(p_1\cdot p_4)(p_2\cdot p_3)]\frac{1}{(p_1-p_3)^2-M_i^2}\frac{1}{(p_1-p_3)^2-M_j^2}. \quad (52)$$

We label the initial state $e^-$ by $(p_1, s_1)$, the initial state $\mu^+$ by $(p_2, s_2)$, the final state $e^-$ by $(p_3, s_3)$, and the final state $\mu^+$ by $(p_4, s_4)$.

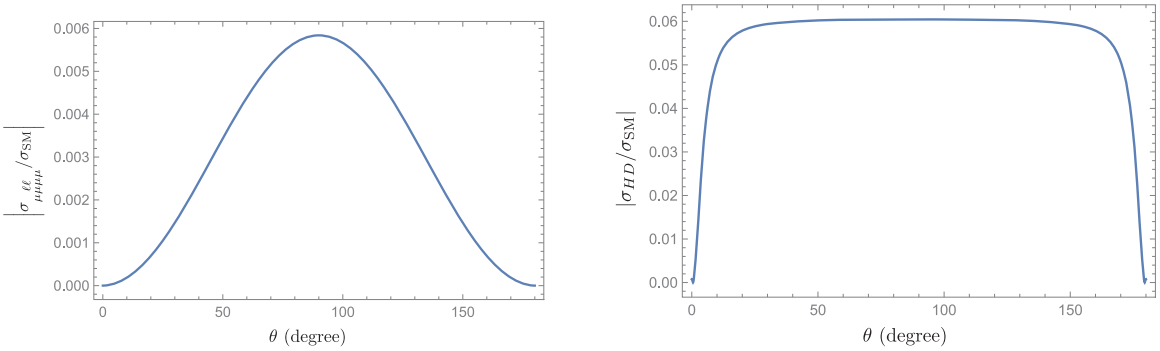


**Fig. 2.** The $\theta$ dependence of the ratio of the new physics contribution to the SM one for $C_{\ell\ell,\mu\mu\mu} = 1/(100\,\text{TeV})^2$ (left) and $C_{HD} = 1/(\text{TeV}^2)$ (right) at the $\mu^+\mu^+$ collider of $\sqrt{s} = 2\,\text{TeV}$. The initial helicity is set to be $s_1 = s_2 = 1$.

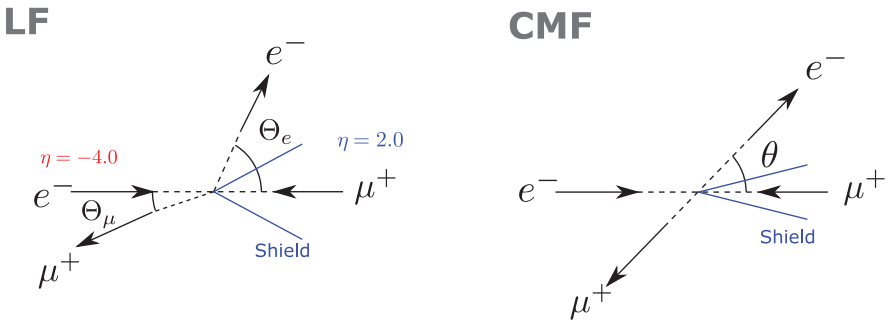


**Fig. 3.** The angular range in which the electron and the muon go in the events we used. The left (right) figure represents the laboratory (center-of-mass) frame.

In this analysis, we use the events where both an electron and a muon are observed in a certain range of angles. We require both the electron and muon to go into the range of about 15.4°–178° in the laboratory frame. This requirement corresponds to setting the range of pseudo rapidity to be $-4 < \eta < 2$ (see Fig. 3). The asymmetric angular region is motivated by the fact that we need to place a shield to protect the detector from decay products of the beam muons [27]. Although the detectability of the muons flying in the direction of the shield depends on the design of the detector, we take a conservative assumption that the particles flying into that angular region are not detected. However, since the produced particles tend to go in a direction of the electron beam side due to the beam energies, this shield does not greatly hinder us from catching events. The practically important factor is how widely we can catch events on the electron beam side. See Fig. 4 for the $\eta_{\text{max}}$ dependence of the bounds on $\Lambda_{HD}$.

In this analysis, we could obtain the histograms concerning both electrons and muons. However, since we expect better angular resolution for electrons, we only use the electron histogram. As a result of the requirement mentioned above, the angular range is determined as $62.8° \lesssim \Theta_e \lesssim 178°$. We summarize the kinematic formulas in Appendix. A.

The constraints we can obtain are summarized in Table 2. We assume the integrated luminosity $\int \mathcal{L} dt = 1\,\text{ab}^{-1}$. It is worth noting that the constraints, apart from on four-fermion operators, are stronger than at the $\mu^+\mu^+$ collider. The $\sqrt{s}$ dependence of the bounds and the $\theta$ dependence of the ratio of the new physics contribution to the SM, respectively, are given in Figs. 5 and 6 for $C_{HD}$.

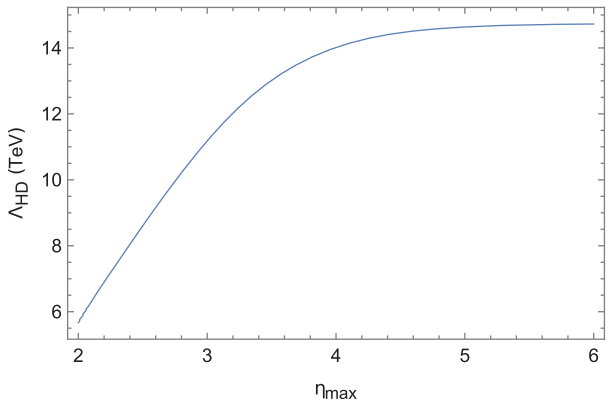


**Fig. 4.** The $\eta$ cut (electron beam side) dependence of the bounds on $\Lambda_{HD}$ for the $e^-\mu^+$ collider of the initial energy $E_e = 30\,\text{GeV}$ and $E_\mu = 1\,\text{TeV}$.

**Table 2.** Constraints on SMEFT operators at the two-sigma level obtained from a $\mu^+e^-$ collider with $E_e = 30$ GeV and $E_\mu = 1$ TeV which amounts to $\sqrt{s} = 346$ GeV. The integrated luminosity is assumed to be 1 ab$^{-1}$. The polarizations of the beams are indicated in the order of $e^-\mu^+$. The bin size for $\Theta_e$ is taken as 1°. We require both muon and electron to go into the range of $15.4^\circ \lesssim \Theta \lesssim 178^\circ$, corresponding to $\eta_{max} = 2$ for the muon beam side and $\eta_{max} = 4$ for the electron beam side. As a result, the angle range of the electron is $62.8^\circ \lesssim \Theta_e \lesssim 178^\circ$.

| | RR | RL | LR | LL |
|---|---|---|---|---|
| $C_{HWB}$ | 6.9 TeV | 24 TeV | 26 TeV | 6.9 TeV |
| $C_{HD}$ | 6.8 TeV | 9.0 TeV | 14 TeV | 6.8 TeV |
| $C_{H\ell}^{(1)}$ | 15 TeV | 0 | 20 TeV | 15 TeV |
| $C_{H\ell}^{(3)}$ | 20 TeV | 18 TeV | 35 TeV | 20 TeV |
| $C_{He}$ | 16 TeV | 19 TeV | 0 | 16 TeV |
| $C_{\ell\ell}$ | 9.6 TeV | 13 TeV | 43 TeV | 9.6 TeV |
| $C''_{\ell\ell}$ | 0 | 0 | 47 TeV | 0 |
| $C_{e\mu}$ | 0 | 66 TeV | 0 | 0 |
| $C_{ee\mu\mu}^{\ell e}$ | 0 | 0 | 0 | 44 TeV |
| $C_{\mu\mu ee}^{\ell e}$ | 44 TeV | 0 | 0 | 0 |

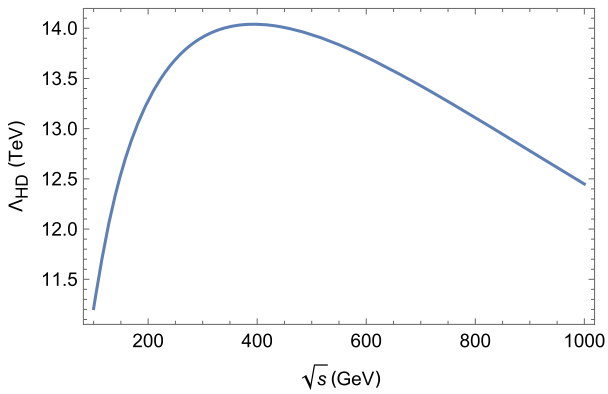


**Fig. 5.** The $\sqrt{s}$ dependence of the bounds on $\Lambda_{HD}$ for the $e^-\mu^+$ collider. The initial helicity is given as $s_1 = -1$, $s_2 = 1$. We assume the constant ratio $E_\mu/E_e = 1000/30$ in drawing the figure.

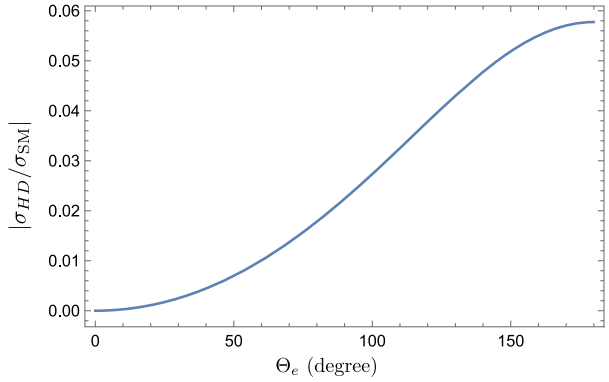


**Fig. 6.** The $\Theta_e$ dependence of the ratio of the new physics contribution to the SM one for $C_{HD} = 1/(\text{TeV}^2)$ for the $e^-\mu^+$ collider. The initial helicity is given as $s_1 = -1$, $s_2 = 1$.

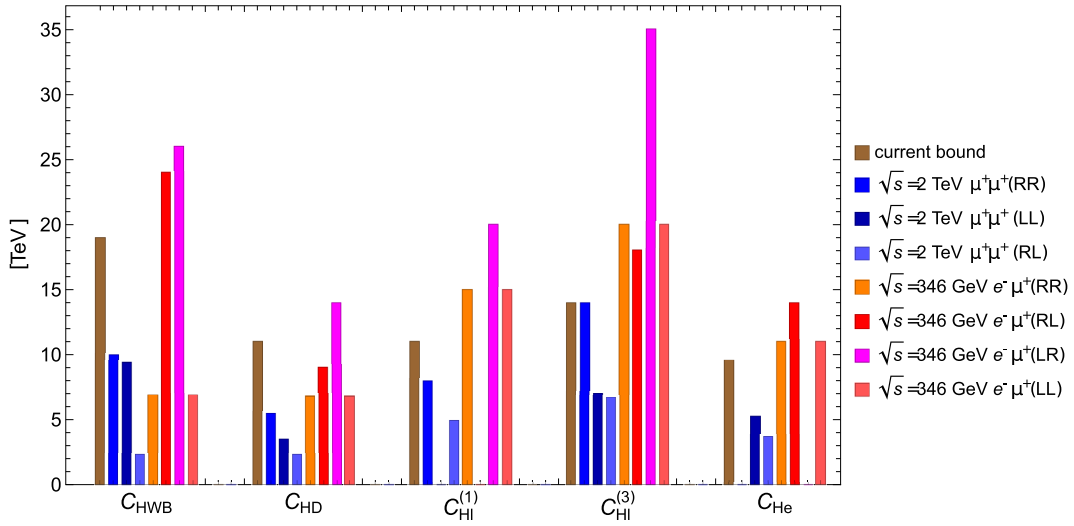


**Fig. 7.** The current constraint and expected constraints from various scattering processes at $\mu$TRISTAN.

## 5. Comparison to the current limits

We compare the above expected constraints with the current constraints. In Figs. 7 and 8, our results are compared with the current bounds given by Table 1 of Ref. [28].[1] Here their "individual" result is referred. Constraints on all the operators relevant to this study are expected to be improved. In particular, constraints on four-fermion interactions can be drastically improved.

The results we obtain can be compared with studies based on other future colliders. For example, in Ref. [29] the future projections of the limits on SMEFT operators are shown under various assumptions of future colliders such as the ILC and the FCC-ee. Obviously, the $\mu$TRISTAN constraints are particularly strong for operators involving muons. The reach of O(100) TeV is made possible by the TeV energy beam of the muons. The four-fermion-type operators make a large contribution to the scattering amplitude at high energies as they are dimension-six operators. On the other hand, operators involving the Higgs field are effectively dimension-four (or less) operators after substituting its VEV, and the contributions do not grow as energy increases, and thus our bounds lay in the range of 10−40 TeV. The corresponding pro-

[1] In Figs. 7 and 8, the current bound, e.g. of 19 TeV for $C_{HWB}$, means that the current (two-sigma level) error size of $C_{HWB}$ is $\delta C_{HWB} = 1/(19\ \text{TeV})^2$.

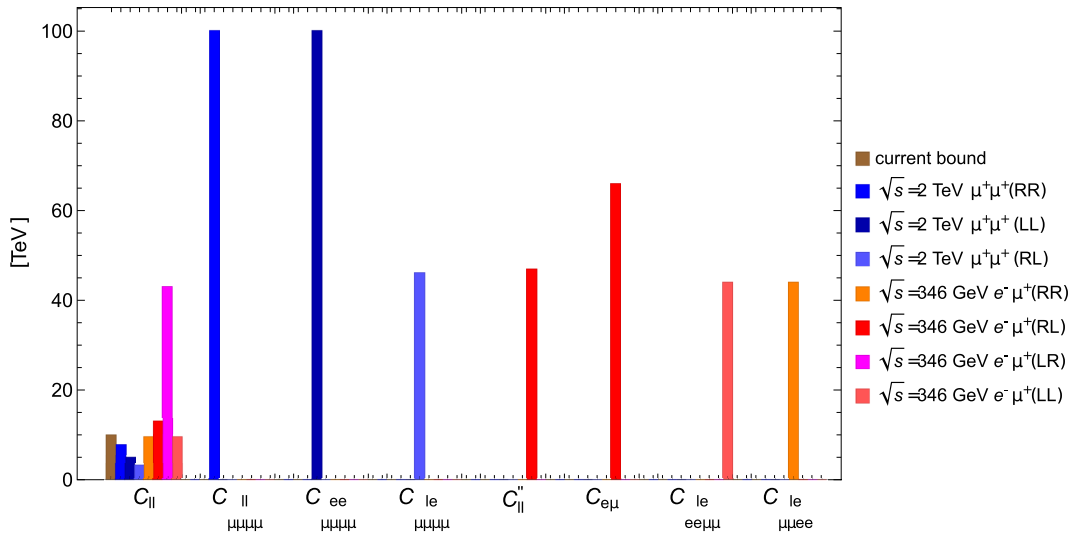


**Fig. 8.** The current constraint and expected constraints from various scattering processes at $\mu$TRISTAN.

jections of the future colliders, ILC and FCC-ee, are similar or better [29]. However, our present study is limited to the elastic scattering experiments of leptons, and other processes may give better constraints. The complete study should include scatterings of W bosons as well as Higgs bosons. We leave those studies for the future.

This work is relevant to studies that explain the recent W boson mass anomaly [30] using SMEFT. Our study shows that the coefficients relevant to the W boson mass formula Eq. (40) can be studied in the scattering processes. In Ref. [28], it is shown that non-zero $C_{HD}$ (with the other coefficients set to zero) may explain the anomaly. In this scenario, $C_{HD}$ was determined as $C_{HD} = -[0.035, 0.019]/(\text{TeV}^2)$ with the error $\delta C_{HD} = 0.012/(\text{TeV}^2)$ at the two-sigma level. Our study shows that the error of $C_{HD}$ can be reduced to $\delta C_{HD} \simeq 0.005/(\text{TeV}^2)$. Therefore, this improvement can show more clearly whether $C_{HD}$ deviates from zero or not. (In addition, we may be able to measure $M_W$ directly at these new collider experiments.)

## 6. Summary

Lepton colliders are known to be sufficiently powerful for precision measurements. There have been extensive discussions of $e^+e^-$, $\mu^+\mu^-$, and $e^-e^-$ colliders as next-generation colliders. In this paper, we studied $\mu^+$-based colliders because realistic muon beams can potentially be achieved much earlier than $\mu^-$ beams by using the technology of ultra-cold muons.

We assumed the energy of the $\mu^+$ beam to be 1 TeV which is discussed as the design parameter of $\mu$TRISTAN [17] with a main ring circumference of 3 km. In the $\mu^+\mu^+$ collider option, we find that one can probe the new physics interactions up to 100 TeV. This means that, for example, the effects of new gauge interactions of the muon can be seen up to the symmetry-breaking scale of $O(100)$ TeV.

We also studied the reach of the $\mu^+e^-$ collider with an electron energy of 30 GeV. This option is motivated by the measurements of the coupling of the Higgs boson, which is copiously produced through the W boson fusion process. We find that running with this energy is also optimal for electroweak precision measurements, and one can improve the constraints for $C_{HWB}$, $C_{HD}$, $C_{Hl}$, and $C_{He}$.

We worked at tree level for the calculation of the SM processes. This is sufficient to approximately understand the potential (best) reach of the new physics scale. However, it would be necessary to sufficiently suppress systematic uncertainties in the SM predictions by performing loop-level calculations for actual analyses and for a more precise estimate of the reach. See, for example, Ref. [31] for recent developments of the SM calculation.

The energy of the muon beam can be much higher for a larger ring. In that case, the sensitivity to four-lepton operators gets much better. For other operators involving the Higgs fields, the modification of the Higgs coupling would be more important at high energy. In addition, one can also hope to find new particles directly. Clearly, the development of muon acceleration technology will be an important key for future particle physics.

**Acknowledgements**

The work is supported by JSPS KAKENHI grant numbers JP19H00689 (R.K., R.M.), JP19K14711 (H.T.), JP21H01086 (R.K.), and JP21J01117 (Y.H.), and MEXT KAKENHI grant number JP18H05542 (R.K., H.T.).

## Funding

Open Access funding: SCOAP[3].

## Appendix A. The laboratory frame coordinates for the $\mu^+e^-$ collider

In the $\mu^+e^-$ collider, we have to note that beam energies are asymmetric. We give some formulae concerning kinematics. In the center-of-mass frame, the momenta are given by

$$p_1 = \frac{\sqrt{s}}{2}\begin{pmatrix}1\\0\\0\\1\end{pmatrix}, \quad p_2 = \frac{\sqrt{s}}{2}\begin{pmatrix}1\\0\\0\\-1\end{pmatrix}, \quad p_3 = \frac{\sqrt{s}}{2}\begin{pmatrix}1\\0\\\sin\theta\\\cos\theta\end{pmatrix}, \quad p_4 = \frac{\sqrt{s}}{2}\begin{pmatrix}1\\0\\-\sin\theta\\-\cos\theta\end{pmatrix}. \tag{A1}$$

The matrix for transforming to the laboratory frame is given by

$$M = \begin{pmatrix}\gamma & 0 & 0 & \beta\gamma\\0 & 1 & 0 & 0\\0 & 0 & 1 & 0\\\beta\gamma & 0 & 0 & \gamma\end{pmatrix}. \tag{A2}$$

That is, the momenta in the laboratory frame are given by $p_1' = Mp_1$ and so on. The boost factor is obtained from

$$E_e = \frac{\sqrt{s}}{2}\gamma(1+\beta), \quad E_\mu = \frac{\sqrt{s}}{2}\gamma(1-\beta), \tag{A3}$$

where $\beta$ is explicitly given by

$$\beta = \frac{1-\frac{4E_\mu^2}{s}}{1+\frac{4E_\mu^2}{s}} = \frac{E_e - E_\mu}{E_e + E_\mu}. \tag{A4}$$

The angle $\Theta_\mu$, in which the final muon goes in the laboratory frame, is given by

$$-\cos\Theta_\mu = \frac{p_{4,z}'}{|\vec{p}_4'|} = \frac{\gamma(\beta-\cos\theta)}{\sqrt{\sin^2\theta+\gamma^2(\beta-\cos\theta)^2}}, \tag{A5}$$

which reads

$$\cos\theta = \frac{-\beta\gamma^2\sin^2\Theta_\mu - \cos\Theta_\mu}{-\gamma^2+\cos\Theta_\mu{}^2(-1+\gamma^2)}. \tag{A6}$$

Then we have

$$\mathrm{d}y = \mathrm{d}\left(\frac{1-\cos\theta}{2}\right) = -\frac{\mathrm{d}(\cos\theta)}{2} = -\frac{1}{2}\frac{\gamma^2 - 2\beta\gamma^2\cos\Theta_\mu + (\gamma^2-1)\cos{\Theta_\mu}^2}{\left(\gamma^2 - (\gamma^2-1)\cos{\Theta_\mu}^2\right)^2}\mathrm{d}(\cos\Theta_\mu). \tag{A7}$$

The angle of the final electron in the laboratory frame, $\Theta_e$, is given similarly as

$$\cos\Theta_e = \frac{p'_{3,z}}{|\vec{p}'_3|} = \frac{\gamma(\beta+\cos\theta)}{\sqrt{\sin^2\theta + \gamma^2(\beta+\cos\theta)^2}}, \tag{A8}$$

from which the following relations can be obtained:

$$\cos\theta = \frac{\beta\gamma^2\sin^2\Theta_e - \cos\Theta_e}{-\gamma^2 + \cos{\Theta_e}^2(-1+\gamma^2)}, \tag{A9}$$

$$\mathrm{d}y = -\frac{1}{2}\frac{\gamma^2 + 2\beta\gamma^2\cos\Theta_e + (\gamma^2-1)\cos{\Theta_e}^2}{\left(\gamma^2 - (\gamma^2-1)\cos{\Theta_e}^2\right)^2}\mathrm{d}(\cos\Theta_e). \tag{A10}$$

## References


[1] S. Schael et al., Phys. Rep. **427**, 257 (2006), hep-ex/0509008 [Search inSPIRE].
[2] The ALEPH, CDF, D0, DELPHI, L3, OPAL, SLD Collaborations, the LEP Electroweak Working Group, the Tevatron Electroweak Working Group, and the SLD electroweak and heavy flavour groups, arXiv:1012.2367 [Search inSPIRE].
[3] S. Schael et al., Phys. Rep. **532**, 119 (2013), arXiv:1302.3415 [Search inSPIRE].
[4] E. Derman and W. J. Marciano, Ann. Phys. **121**, 147 (1979).
[5] A. Czarnecki and W. J. Marciano, Phys. Rev. D **53**, 1066 (1996), hep-ph/9507420.
[6] M. J. Ramsey-Musolf, Phys. Rev. C **60**, 015501 (1999), hep-ph/9903264.
[7] A. Czarnecki and W. J. Marciano, Int. J. Mod. Phys. A **15**, 2365 (2000), hep-ph/0003049.
[8] P. L. Anthony et al., Phys. Rev. Lett. **95**, 081601 (2005), hep-ex/0504049.
[9] K. S. Kumar, S. Mantry, W. J. Marciano, and P. A. Souder, Ann. Rev. Nucl. Part. Sci. **63**, 237 (2013), arXiv:1302.6263 [Search inSPIRE].
[10] J. Benesch et al., arXiv:1411.4088 [Search inSPIRE].
[11] W. Buchmuller and D. Wyler, Nucl. Phys. B **268**, 621 (1986).
[12] B. Grzadkowski, M. Iskrzynski, M. Misiak, and J. Rosiek, J. High Energy Phys. **10**, 085 (2010), arXiv:1008.4884 [Search inSPIRE].
[13] I. Brivio and M. Trott, Phys. Rep. **793**, 1 (2019), arXiv:1706.08945 [Search inSPIRE].
[14] J. Ellis, M. Madigan, K. Mimasu, V. Sanz, and T. You, J. High Energy Phys. **4**, 279 (2021), arXiv:2012.02779 [Search inSPIRE].
[15] Ties Behnke et al., arXiv:1306.6327 [Search inSPIRE].
[16] J. Ellis and T. You, J. High Energy Phys. **3**, 089 (2016), arXiv:1510.04561 [Search inSPIRE].
[17] Y. Hamada, R. Kitano, R. Matsudo, H. Takaura, and M. Yoshida, Prog. Theor. Exp. Phys. **2022**, 053B02 (2022), arXiv:2201.06664 [Search inSPIRE].
[18] Y. Kondo et al., in Proc. IPAC'18, eds. Shane Koscielniak, Todd Satogata, Volker RW Schaa, and Jana Thomson (JACoW Publishing, Geneva, 2018), pp. 5041–5046.
[19] M. Abe et al., PTEP **2019**, 053C02 (2019), arXiv:1901.03047 [Search inSPIRE].
[20] M. E. Peskin and T. Takeuchi, Phys. Rev. Lett. **65**, 964 (1990).
[21] G. Altarelli and R. Barbieri, Phys. Lett. B **253**, 161 (1991).
[22] R. Alonso, E. E. Jenkins, A. V. Manohar, and M. Trott, J. High Energy Phys. **04**, 159 (2014), arXiv:1312.2014 [Search inSPIRE].
[23] G. W. Bennett et al., Phys. Rev. Lett. **89**, 101804, (2002), [Erratum: Phys. Rev. Lett. 89, 129903 (2002)], hep-ex/0208001.
[24] G. W. Bennett et al., Phys. Rev. Lett. **92**, 161802 (2004), hep-ex/0401008.
[25] G. W. Bennett et al., Phys. Rev. D **73**, 072003 (2006), hep-ex/0602035.
[26] B. Abi et al., Phys. Rev. Lett. **126**, 141801 (2021), arXiv:2104.03281 [Search inSPIRE].
[27] N. Bartosik et al., J. Instrum. **15**, P05001 (2020), arXiv:2001.04431 [Search inSPIRE].

[28] E. Bagnaschi, J. Ellis, M. Madigan, K. Mimasu, V. Sanz, and T. You, J. High Energy Phys. **08**, 308 (2022), arXiv:2204.05260 [Search inSPIRE].
[29] J. De Blas, G. Durieux, C. Grojean, J. Gu, and A. Paul, J. High Energy Phys. **12**, 117 (2019), arXiv:1907.04311 [Search inSPIRE].
[30] T. Aaltonen et al., Science **376**, 170 (2022).
[31] S. G. Bondarenko, L. V. Kalinovskaya, L. A. Rumyantsev, and V. L. Yermolchyk, arXiv:2203.10538 [Search inSPIRE].